Lateral Optical Sensor With Slip Detection for Locating Live Products on Moving Conveyor

Kok-Meng Lee, *Fellow, IEEE*, and Shaohui Foong, *Student Member, IEEE*

***Abstract*—This paper presents a method to determine the 2-D profile and motion of a live product (such as chicken for poultry meat processing) on a moving conveyor from a lateral optical sensor that consists of an orthogonal pair of line array (LA) scanners. Unlike most line array (LA) scanners designed to provide a 2-D image of a static object, the lateral optical sensor presented here offers a practical means to detect object slippage on the conveyor in real time. Three examples are given to illustrate the effectiveness of this sensing method. The first simulates the 2-D boundary of a geometrically well-defined object on an accelerating conveyor, which offers intuitive insights on the effects of conveyor dynamics and object slippage on the accuracy of the 2-D boundary measurement. The second experimentally demonstrates the extendibility of LA sensors to detect both engineering and natural objects. The final example illustrates the application of the lateral optical sensor as a real time feedback sensor for active singulation of natural objects.**

***Note to Practitioners*—This paper was motivated by the problem of automated handling of live chickens on moving conveyors for poultry meat processing. The method presented here can also apply to other object handling applications where the absolute location of the randomly shaped moving object is used as a triggering signal for subsequent operation. Existing approaches generally rely on the use of the conveyor speed with a beam switch (or a line scan array) and are unable to account for object slippage or voluntary motion. This paper suggests a new approach using a pair of orthogonal optical line sensors along with the known conveyor speed to determine the absolute location and lateral profile of the object on the moving conveyor; both engineering and natural objects are considered. In this paper, we formulate a locating method that exploits the fast scan rate of photoelectric sensors to detect discrepancies between the position/velocity of the object and the conveyor. We then illustrate how this information can be used to compensate for object slippage due to conveyor acceleration and perform object-based location calibration. Preliminary physical experiments conducted on a small number of live chickens using (300 mm-long) line sensors (consisting of 128 emitter/receiver pairs spaced at 2.5 mm) sampled at a rate of 40–50 ms suggest that this method has a significant potential in applications such as active singulation where object injuries due to unpredictable voluntary motion must be minimized.**

***Index Terms*—Food processing, object handling, sensor, slip detection.**

Manuscript received June 27, 2008; revised November 17, 2008 and April 22, 2009. First published September 09, 2009; current version published January 08, 2010. This paper was recommended for publication by Associate Editor L. Dong and Editor V. Kumar upon evaluation of the reviewers' comments. This work was supported in part by the Georgia Agricultural Technology Research Program and in part the U.S. Poultry and Eggs Association.

The authors are with the Woodruff School of Mechanical Engineering, Georgia Institute of Technology, Atlanta, GA 30332-0405 USA (e-mail: kokmeng.lee@me.gatech.edu; shao@gatech.edu).

Color versions of one or more of the figures in this paper are available online at http://ieeexplore.ieee.org.

Digital Object Identifier 10.1109/TASE.2009.2025505

I. Introduction

LINE scanners, widely used in document reproduction, are well known for their ability to offer high-resolution images with inexpensive sensors in limited viewing distance. However, their applications for industrial automation are under exploited. In applications such as part-presentation on moving conveyors, real-time positional information is essential for subsequent robotic or automated mechanical handling. Motivated by practical problems commonly encountered in food processing where natural objects must be handled repetitively at high-speed, this paper introduces a new method (referred to here as a lateral optical sensor) to detect and compensate for object slippage on the conveyor, while reconstructing the object boundary in real time. To facilitate the illustration, we present this sensing method in the context of mechanical singulation.

Conventional singulating systems [1], [2], which involve the separation of randomly spaced objects in order to maintain a minimum specified distance between neighboring objects, are commonly passive. They remain in constant-speed motion as the arrival conveyor moves object after object through two symmetrical sets of continuously rotating fingers. Active singulation, which requires only a small number of finger-sets, not only eliminates excess movement when the object is not completely in the specified region (or there are no objects to be singulated), but also objects can be more accurately spaced on the next conveyor as contact forces on the object can be more consistently predicted. More importantly, in handling of live objects where flexible fingers are commonly used to accommodate a limited range of varying sizes and shapes [2] regardless of their orientation, active singulation effectively minimizes visual stimuli of the rotating fingers and thus could drastically reduce injuries due to unpredictable escape behaviors. The success of active singulation, however, relies heavily on the ability to detect the arrival of the objects and estimate the spacing between incoming object in order to manipulate the speed of the singulator and conveyors.

The simplest scheme to activate the singulating fingers when an object enters the specified region is to use a point proximity sensor. Unlike engineering objects which have well-defined boundary with geometrically simple edges or curves, natural objects (such as food and live products for meat processing) do not have a well-defined shape. As a result, the activation of the point sensor is generally inconsistent due to the irregularity of the body shape, and the possibility of object slippage or voluntary motion (in the case of live products). Any accidental activation of the point sensor will cause the singulation system to activate earlier than expected.

While commercial cameras are capable of capturing 2-D images of irregularly shaped objects and features [3], [4], there

are tradeoffs between the image resolution and the field-of-view (FOV), which depends on the viewing distance and illumination considerations. In handling automation of food and/or live products, shadows, highlights and perspective distortion due to shape and color irregularities are common problems in images captured on a camera [5], [6]. Particularly when products must be singulated in parallel conveyors to feed a processing line at high-speed, the use of cameras that require a minimum viewing distance is often impractical for capturing unblocked, distortion-free side-views. These, along with their comparatively slow sampling rates for 2-D image processing, often impede their implementation in real-time control for handling live-product.

A potential alternative to overcome the shortcomings of a point sensor or a 2-D imaging sensor for active singulation is to use a line sensor. Line sensors have been used as a lateral position detection device to detect lane markers on roads [7] for applicative use in autonomous navigation. The rapid scanning of the line sensor estimates both the heading and position of the car within the lane markers. In biometrics, small scale line sensors are implemented within a fingerprint verification system [8]. In addition, an array of PIN photodiodes can be used as a depth measurement tool to obtain a 3-D topological image [9]. In the preceding applications, the line sensors are mobile while the objects of interest are stationary and the general emphasis is obtaining a 2-D image of the static objects. Measurements of dynamic objects are possible using a single-line CCD camera that measures the spin rate of a specially marked golf ball as it passes the stationary sensor [10]. Similarly, accurate velocity estimation of automobiles at speeds up to 120 km/h was achieved using a high-speed dual-line sensor system [11] through monitoring the time between detection of the same feature by each line sensor. The fidelity of the line-sensor-based measurement often relies on the assumption of nonslip conditions. Slip detection is an essential process in many industrial applications. It is used extensively to ensure mobility and continued functionality of all-terrain vehicles [12], [13] by actively monitoring wheel angular speeds using specialized angular sensors. Nonconventional methods of slip detection that do not require velocity sensors include scrutinizing current input into driving motors [14] and using tactile and force feedback sensors [15].

For the above reasons, we develop a method based on a combination of optical line-array sensors for active singulation where lateral movements of the objects are constrained and thus relatively insignificant as compared to the spacing between incoming objects on a moving conveyor. The remainder of this paper offers the following:

1) We present a lateral optical sensor to construct the 2-D boundary of a natural object on a moving conveyor from discrete profile scans. This sensor, which uses a pair of line array scanners mounted perpendicularly, exploits the fast scan rate of the photoelectric sensors to detect discrepancies between the position/velocity of the object and the conveyor. While this method is similar to a flatbed scanner for 2-D document reproduction in that distortion-free profiles can be obtained in tight physical space, we extend the line scan method to derive the 2-D profile of a 3-D moving object. This paper represents among the first to demonstrate the advantage of line-sensors for applications where live products must be singulated in parallel conveyors to feed a processing line at high-speed.
2) We relax the nonslip assumption in the direction of conveyor motion, and offer a practical means to detect and compensate for object slippage in the direction of conveyor motion) to perform object-based location calibration.
3) To demonstrate the effectiveness of this method, we offer three illustrative examples. The *first* example numerically illustrates the effects of conveyor dynamics and object slippage due to conveyor acceleration through comparisons of the reconstructed side profiles of a well defined geometrical object. The *second* example investigates experimentally the extendibility of LA sensors to detect both engineering and natural objects. Specifically, experiments were conducted on a moving platform which simulates an automated handling system of live broilers (meat chickens). The *third* example examines the feasibility of implementing this method in a process of active singulation in an automated natural object handling application. Key issues include maintaining object throughput and precise triggering.

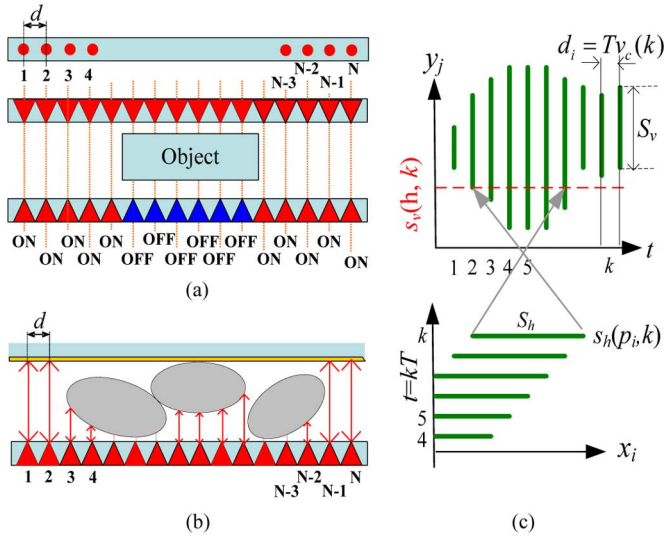

Fig. 1. Optical Line Sensor. (a) Binary LAH sensor (plan view). (b) Gray-level LAH sensor (plan view). (c) $s_v(y_j, k)$ and $s_h(x_j, k)$.

II. Optical Line Array (LA) Sensors

An emitter-receiver pair (a point sensor) is similar to an on–off switch which is said to be "on" if the light beam from the emitter is collected unobstructed by the receiver. The LA sensor consists of N photoelectric sensors (or emitter–receiver pairs) equally spaced along a straight line at distance d (which defines the sensor resolution), as shown in Fig. 1(a) and (b). The emitters are pulse modulated at preset frequencies to prevent corruption from adjacent emitters and ambient light.

The LA sensor may be installed in vertical (LAV) and horizontal (LAH) configurations.

- LAV: Placed vertically (perpendicular to the moving surface), a side profile of the object is scanned as it passes between the emitter-receiver pair. The upper time-plot in

Fig. 1(c) shows an example data set captured by the LAV, where the data is a mirror image of the actual object.

- LAH: Mounted at a height h above (and parallel to) the moving surface, the LA sensor captures an instantaneous snapshot of the object length at every time step as shown in the lower time-plot of Fig. 1(c). At this height h, the object is scanned redundantly by the LAH and LAV (when they are fixed relative to each other), the two arrows in Fig. 1(c) illustrate the correspondence between the two time-plots.

A. Sensor Formulation

The status of the ith pixel p_i on the LA sensor at $t = kT$ (where k is an integer and T is the sampling time) can be written as

$$s(p_i,k)=\begin{cases}0 & \text{if beam was made}\\ g & \text{if beam was blocked}\end{cases}\qquad 1\le i\le N. \tag{1}$$

Without loss of generality, we assume that the sensor is binary ($g = 1$). The principle discussed in this paper can be applied to gray-level sensor once an appropriate threshold is determined and normalized.

For an object within the sensing range of a LA sensor, the leading edge E_L of the object can be located by testing the neighbors of the ith pixel

$$\text{If } s(p_m,k)=\begin{cases}0 & i<m<i+\beta\\ 1 & i-\beta<m\le i\end{cases}\quad \text{then } E_L(k)=i \tag{2a}$$

where m is a neighbor point; and β is an integer threshold to be defined. This 0-to–1 transition provides a means to locate the first beam blocked by the object when it enters the detectable region of a LAH. Similarly, the location of the trailing edge E_T is found by using a neighbor point n as follows:

$$\text{If } s(p_n,k)=\begin{cases}1 & i<n<i+\beta\\ 0 & i-\beta<n\le i\end{cases}\quad \text{then } E_T(k)=i. \tag{2b}$$

The trailing edge is a 1-to-0 transition that signals the last beam blocked by a (completely filled) object. An odd number of edge transitions indicates an object enters or leaves the LAH detectable region; a sequence that begins with a leading edge signals an object is entering while that ends with a trailing edge signals the object is leaving.

The span S (or the number of pixels between a leading edge and a trailing edge) can be written as

$$S(k)=E_{L/T}(k)-E_{T/L}(k)+1 \tag{2c}$$

where the subscripts "L/T" and "T/L" denote the E_L-to-E_T transition and the E_T-to-E_L transition, respectively. The span is the continuous beams blocked between E_L and E_T inclusive. A vertical span S_v sequence, which can be obtained from the LAV, gives the object boundary and/or the space above and below the object). The horizontal span S_h (obtainable directly from the LAH) can be used to determine an object's cross sectional length and/or spacing between two adjacent objects. Both S_v and S_h are illustrated in Fig. 1(c).

LA in Vertical Configuration: The side profile can be reconstructed using successive scans of the object as it passes the LAV on a moving conveyor. For a small sampling time T, the object velocity may be assumed to be constant between each scans

$$v(t)\approx v(k)\quad \text{when } kT\le t<(k+1)T. \tag{3}$$

The 2-D image $\mathbf{P}(\mathrm{x},\mathrm{y})$ can be constructed from the LAV data with elements given by (4a, b)

$$x_i\approx\hat{x}_i=v_c(i)T \tag{4a}$$

and

$$P(x_i,y_j)=s_v(y_j,i) \tag{4b}$$

where $v_c(k)$ is the conveyor velocity; and i and j are the x and y pixel indexes of the image $\boldsymbol{P}$. The image fidelity obtained with (4a) and (4b), however, relies on the two assumptions: 1) The conveyor speed $v_c(k)$ is known and T is small; and 2) the object does not move or slip relative to the conveyor.

LA in Horizontal Configuration: Since the spacing between two adjacent columns is velocity dependent, the repetitive LAH snapshots offer a means to measure the absolute velocity of the object (in the direction parallel to the LAH) as it traverses through the LAH by tracking the motion of the leading or trailing edge between two consecutive snapshots. As a second-order approximation, the estimated object velocity $\tilde{v}(k)$ can be estimated from the time derivative of the leading (or trailing) edge motion between consecutive instants

$$\tilde{v}(k)=\dot{E}_{L/T}\approx[3E_{L/T}(k) -4E_{L/T}(k-1)+E_{L/T}(k-2)]d_x/2T \tag{5}$$

where d_x is the spacing between adjacent pixels of the LAH. Moreover, the ability to observe discrepancies between the object velocity and the conveyor velocity allows the detection of slipping between the object and conveyor in the direction of conveyor motion as observed from the LAH. Slipping is said to occur at time k if the conveyor velocity differs from the object velocity

$$|v_c(k)-\tilde{v}(k)|>v_m \tag{6}$$

where v_m is a specified nonzero threshold.

Object-Based 2-D Image Calibration: The "object-based location calibration" is a method for simultaneously locating the object and capturing its 2-D boundary. For applications where objects may slip on the conveyor, the spacing between two adjacent LAV column data depends not only on the conveyor speed but also on the object velocity, which necessitates an LAH/LAV configuration. The following assumptions are made in this method.

1) The conveyor speed is measurable and known; this assumption allows slipping to be detected from (6).
2) The LAH detects the leading and trailing edges of the object before LAV begins and ends its line-scan. As illustrated in Fig. 2(a), if LAV scans the object before LAH detects the first leading edge $E_L(k)$, there will be no basis to estimate the spacing between LAV columns scanned before $t = kT$. However, if LAH leading edge is tracked before LAV makes its first scan (Fig. 2(c)), the LAH edge

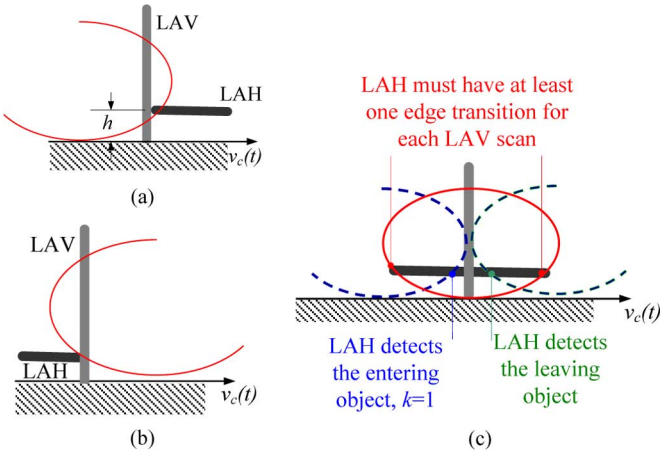

Fig. 2. Side view.

transitions $E_L(t \geq kT)$ can then be used to estimate every spacing between columns scanned by LAV. Similar argument applies to the trailing edge [Fig. 2(b) and (c)].

3) The LAH and LAV are fixed relative to each other; and there is at least an LAH edge transition (leading or trailing) when the LAV makes a scan. This guarantees that every space between LAV-scanned columns can be estimated.

As illustrated in Fig. 1(c), both the LAV and LAH sensors construct a binary image that increases in size with time. The two images have different dimensions but can be related to each another by virtue of their geometric configuration, and the knowledge of sampling interval T and conveyor velocity $v_c(t)$.

1) The pixel values registered in the LAH are repetitions of the $\text{int}(h/d_y)$th pixel of the LAV

$$s_h(p_i, k) = s_v[\text{int}(h/d_y), \text{int}(T_d/T) + (k - i)] \tag{7a}$$

where $T_d = d_s/v(0)$.

2) The span S_h given by (2c) provides an instantaneous snapshot by the LAH, which can also be obtained from the LAV data but is velocity dependent as it must be deduced from data of more than one vertical scans

$$\hat{S}_h = \text{int}\left\{\frac{T}{d_x}\sum_{i=1}^{l} v_c(i)\right\} \tag{7b}$$

where ℓ is the number of sampling periods between the leading and trailing edges on the LAV at a specified height h [Fig. 1(c)].

B. Data Representation

Unlike conventional line proximity sensors which only detect if any of the light beams are blocked as the sole binary (digital) output, we introduce here a hybrid scheme to utilize a combination of digital and analog output signals as a function of the individual instantaneous beam-states to convey a variety of measurements and information. Such signals are preferred as they can be directly integrated in existing control schemes in motion controllers as a triggering device (digital output) or independent measurement sensor (analog output) as compared to transmitting individual beam states that require further processing by a computer.

TABLE I
EXAMPLE LAV DATA $s_h(p_i, k)$

$k=$	1	2	3	4	5	6	7	8
p_8	0	0	0	1	1	0	0	0
p_7	0	0	1	1	1	1	0	1
p_6	0	1	1	1	1	1	1	1
p_5	1	1	1	1	1	1	1	1
p_4	1	1	1	1	1	1	1	0
p_3	**0**	**1**	**1**	**1**	**1**	**1**	**0**	**0**
p_2	0	0	1	1	1	1	0	0
p_1	0	0	0	1	1	0	0	0
Hex	18	3C	7E	FF	FF	7E	38	70
E_L	5	6	7	–	–	7	6	7
E_T	4	3	2	–	–	2	4	5
S_v	2	4	6	–	–	6	3	3

TABLE II
EXAMPLE LAH $s_h(p_i, k), G = 1$ (BINARY)

k	p_1	p_2	P_3	p_4	p_5	p_6	P_7	p_8	Hex	E_L	E_T	S_h
13	0	0	0	0	0	0	0	0	00	0	0	0
12	0	0	0	0	0	0	0	1	01	–	8	–
11	0	0	0	0	0	0	1	1	03	–	7	–
10	0	0	0	0	0	1	1	1	07	–	6	–
9	0	0	0	0	1	1	1	1	0F	–	5	–
8	0	0	1	1	1	1	1	0	3E	7	3	5
7	0	1	1	1	1	1	0	0	7C	6	2	5
6	1	1	1	1	1	0	0	0	F1	5	–	–
5	1	1	1	1	0	0	0	0	F0	4	–	–
4	1	1	1	0	0	0	0	0	E0	3	–	–
3	1	1	0	0	0	0	0	0	C0	2	–	–
2	1	0	0	0	0	0	0	0	A0	1	–	–
1	0	0	0	0	0	0	0	0	00	–	–	–

The individual binary states of the LA sensors can be represented in the hexadecimal (Hex) system using one character $(0 \ldots \text{F})$ to register the states of the 4 pixels. Tables I and II show an example displaying the beam states of a 8-pixel LAV/LAH pair along with their HEX representation and measurement features. Table I tabulates the LAV data, where each column line-scans the passing object vertically. On the other hand, the beam-states of the LAH (collinear with the 3rd beam of the LAV) are given in Table II showing the horizontal snapshots.

III. Simulation and Experimental Results

Two distinct examples are given here to illustrate the optical method for slip detection and to offer intuitive insights into the LA based sensors.

- The first example presents a simulated environment in which a well-defined geometrical object slips on a moving conveyor. The importance of detecting slipping of objects is demonstrated by comparing various methods of constructing a 2-D boundary image of an object undergoing slipping.
- The second example illustrates experimentally the extendibility of LA sensors to detect both engineering and natural objects. Specifically, experiments were conducted on a moving platform which simulates an automated handling system of live broilers (meat chickens).

A. Slip Detection Example—Numerical Simulation

Slipping would result in velocity discrepancies between the object and the conveyor. If there is insufficient friction between

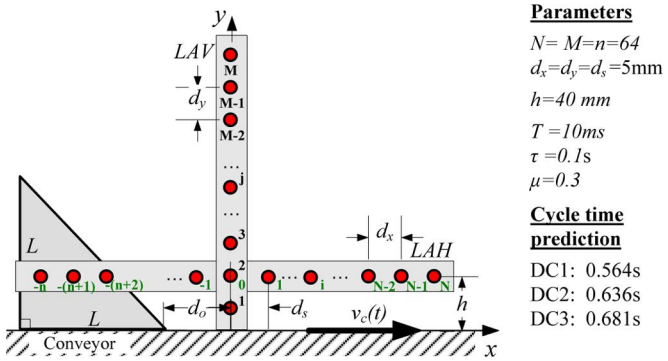

Fig. 3. Schematics illustrating Example 1.

the object and conveyor surface, slipping will occur when the conveyor acceleration exceeds a critical value

$$a_c = \mu g \tag{8}$$

where μ is the coefficient of friction between the object and the conveyor surface. We illustrate an example (Fig. 3) to offer some insight to the effects of slip in addition to the following factors on the accuracy of the optical LA sensor pair: 1) the variation of conveyor speed and 2) the unknown object velocity relative to the conveyor.

Fig. 3 shows the (right-angled triangular) test-object on the conveyor (which travels initially at a constant velocity, and then uniformly accelerates to a specified higher velocity) as the object passes through the sensor pair. The conveyor dynamics is assumed to be first order of the form

$$\tau dv_c/dt + v_c(t) = u(t) \tag{9}$$

where τ is the time constant and $u(t)$ is the normalized controlling input to the conveyor.

A MATLAB program was written to simulate the data representation of the LAH/LAV sensor pair. We study the effects by comparing the results against two common alternative design configurations (DCs). In all cases, the conveyor speed increases from its initial 0.3 to 1.2 m/s after 40 time steps. The three DCs are configured as follows.

- *DC-A*: A nonslip condition between object and conveyor is assumed; $v(t) = v_c(t)$. The conveyor speed is not measured but equal to its specified step input.
- *DC-B*: As in *DC-A*, the nonslip condition is assumed. However, an encoder measures the conveyor speed and a point sensor locates the first leading edge, E_T, but does not have the ability to track its motion.
- *DC-C*: The object and conveyor velocities, $v(t)$ and $v_c(t)$, are independently measured to detect the condition of slip. The LAH/LAV sensor pair is used to estimate the velocity of the object and reconstruct its image.

In all three DC's, an LAV sensor is used to construct the image of the object. Other parameters used in the simulation are given in Fig. 3; the values characterizing the sensors are based on the technical specification of an off-the-shelf high resolution line sensor manufactured by Banner Engineering Corp. [17]. The results are summarized in Fig. 4.

Fig. 4(a) and (b) compare the velocity and displacement of the object among the three DC's. By locating the trailing edge of the LAV at each sampling instant, the boundary of a mirrored 2-D image $\mathbf{P}(\mathrm{x}, \mathrm{y})$ of the test object can be obtained. Fig. 4(c) compares the image boundary computed using (4a) and (4b) against those taking into account the conveyor dynamics (9) and the conditions of slipping (6) and (8). The computed boundary is mirrored because the profile is incrementally constructed. The resulting timing errors in the x direction as defined below are summarized in Fig. 4(d)

$$\text{error}(k) = |x(k) - \hat{x}(k)|$$

where

$$\hat{x}(k) = T\sum_{i=0}^{k-1} \tilde{v}(i).$$

Some observation can be made from the comparison.

- Provided that the object does not slip, the object displacement can be deduced from (4a) and (4b). However, *DC-A* does not take into account the conveyor dynamics during acceleration; the x-positional error grows as the object accelerates with the conveyor. This results in a geometrically distorted 2-D image in *DC-A*.
- *DC-B* uses the conveyor velocity to estimate the spacing between the LAV column scans. The failure to detect slipping between the object relative to the conveyor surface leads to a constant steady state error in the 2-D image constructed in *DC-B*.
- In *DC-C*, the absolute velocity of the object can be estimated using (5). In addition, the location and duration of slipping can be obtained by comparing the LAH estimated velocity of the object and the measured conveyor velocity using (6). The LAH estimated velocity (5) can be applied to correct profiles (4a) and (4b) that have been distorted by slipping or relative motion of the object as well.

In summary, the LAH offers a practical means to estimate the absolute velocity, detect slipping, and correct the 2-D image boundary of the object. These attractive features offered by a LAH/LAV sensor pair can neither be obtained from a point sensor nor a single LAV sensor.

B. Live Object Location—Experimental Investigation

Unlike engineering objects, live objects such as broilers react actively to the surrounding environment. Abrupt changes such as motion, lighting effects and noise invoke both voluntary and involuntary responses from broilers. For processing of meat products, there is a need to measure the absolute motion of the live object on the moving surface. An experimental investigation was carried out to study the feasibility of utilizing LA sensors for automated handling of live objects on a moving surface undergoing vibratory motion, particularly due to the effect of acceleration.

Experimental Setup: The experimental study [Fig. 5(a) and (b)] was performed on a platform (mass m_p) traveling on a pair of translational bearings (damping coefficient c). The platform (attached between two identical springs of stiffness k) can be modeled analytically as a mass-spring-damper system

$$(m_p + m_b)\ddot{x}(t) + c\dot{x}(t) + 2kx(t) = 0; x(0) = x_o, \dot{x}(0) = 0 \tag{10}$$

where m_b is the mass of the broiler so that the broiler reaction to the initial acceleration

$$\ddot{x}(0) = \omega_n^2 x_o = [2k/(m_p + m_b)]x_o \tag{10a}$$

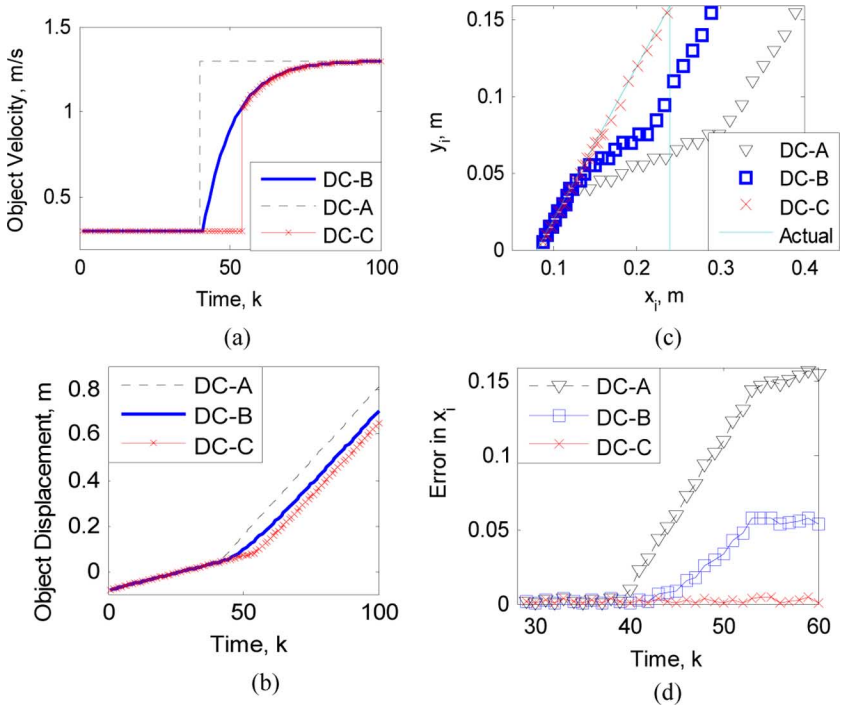

Fig. 4. Simulated results of Example 1. (a) Velocity, (b) displacement, (c) 2-D object boundary, and (d) 2-D error.

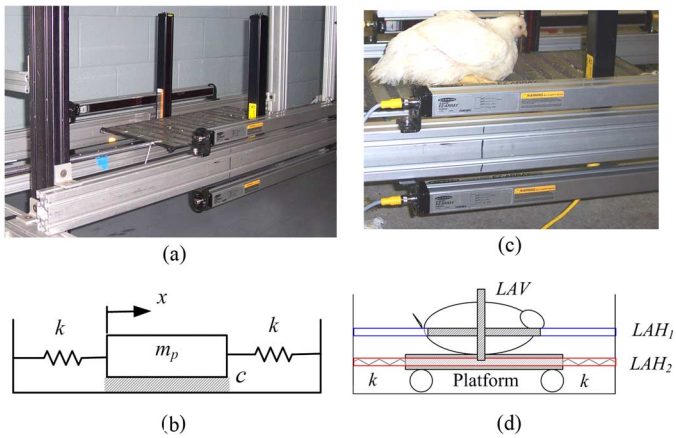

Fig. 5. Experimental setup. (a) Moving platform. (b) Equivalent model. (c) Live broiler. (d) Sensor placement.

TABLE III
DESCRIPTION OF LA SENSORS AND COMMUNICATION

	Beams		Model [16][17]	
	No.	Spacing (mm)	Emitter	Receiver
$LAH_{1,2}$	120	5	EA5E600Q	EA5R600NIXMODQ
LAV	128	2.5	MAHE13A	MAHR13A

Communication interface [18][19]
Programmable gateway (Model: BL20-PG-EN)
Analog I/O unit (Model: BL20-4AI-U/I)

Electrical schematics

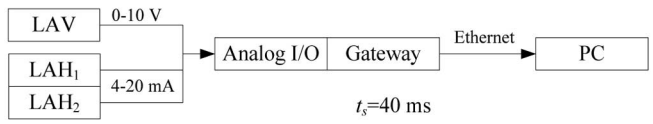

can be studied, and the LA sensor measurements can be validated against the closed-form solution

$$x(t) = x_o e^{-\xi\omega_n t}\frac{1}{\sqrt{1-\xi^2}} \times \sin[(\omega_n\sqrt{1-\xi^2})t + \cos^{-1}\xi] \tag{10b}$$

where

$$2\xi\omega_n = c/(m_p + m_b) \tag{10c}$$

$$\omega_n^2 = 2k/(m_p + m_b). \tag{10d}$$

As shown in Fig. 5(c) and (d), the absolute motions of the object and platform are measured, respectively, by the LAH_1 and LAH_2, while the LAV records the broiler vertical profile. The LAH_2 computes the leading edges of two identical square (3×6 mm^2) rods mounted on the underside of the platform at both ends while the LAH_1 tracks the location of the leading and trailing edges of the object on the platform. The platform position is obtained by averaging the leading edges of the two rods when both rods are in range of the sensor or using only one edge when the other rod is out of range.

The absolute beam positions of the leading and trailing edges (as measured on the LA sensors, each of which consists of an emitter and a receiver) are transmitted as analog outputs of 4–20 mA for the two identical LAHs, and 0–10 V for the LAV. A programmable gateway with an analog I/O unit attached from is used as an interface to record the analog measurements onto a desktop PC via an Ethernet connection at a sampling rate of $t_s = 40$ ms. The description of the LA sensors and communication are summarized in Table III.

Sensor Accuracy Determination: To quantify the accuracy, the LA sensor determined position and velocity were compared to known displacement (with resolution of 0.08 cm) and velocity

TABLE IV
POSITION, VELOCITY, AND ACCELERATION ERROR STATISTICS

Absolute Error	x		v	a
(50 measurements)	cm	pixels	cm/s	m/s^2
Mean	0.144	0.288	3.574	0.525
Standard Deviation	0.091	0.182	2.043	0.491
Max	0.376	0.753	12.436	2.082
Min	0.011	0.023	0.105	0.010

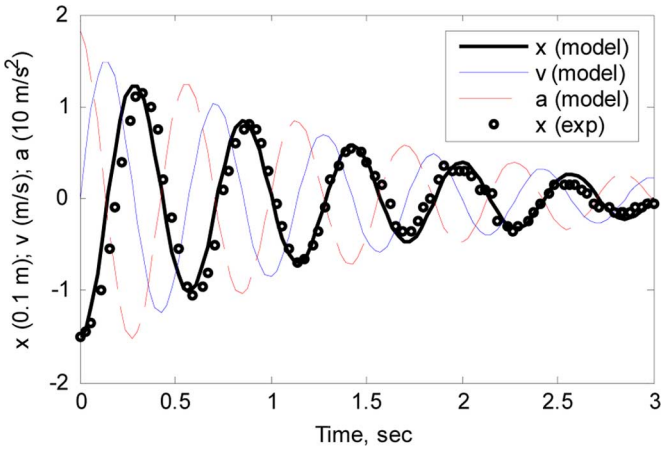

Fig. 6. Experimental results for system identification.

TABLE V
PARAMETERS AND THEIR VALUES USED IN THE EXPERIMENTS

m_p (kg)	c (Ns/m)	k (KN/m)	m_b (kg)
2.1945	2.9317	0.267	1.5471

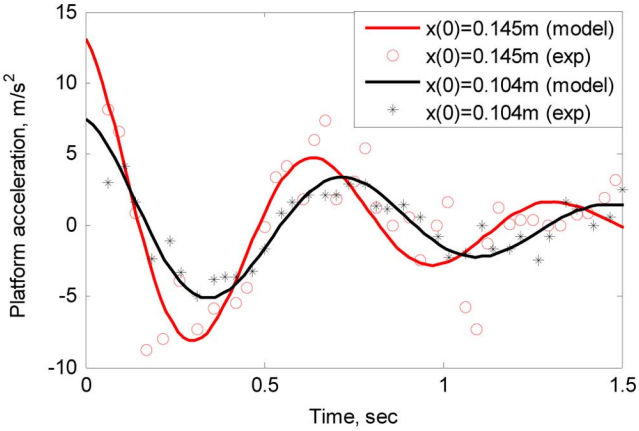

Fig. 7. Comparisons between measured and modeled acceleration.

(measured using a tachometer with resolution of 0.01 cm/s). Acceleration was verified from the time derivative of velocity. The mean and standard deviation of the absolute errors are tabulated in Table IV, where a total of 50 measurement sets were compared.

In Table IV, the position error between the LAH_2 and the known is measured in cm and the number of pixels (beam spacing). To determine the velocity and acceleration errors, a DC motor with an applied step input was used to accelerate the platform along the bearings from rest to a steady-state speed of 40 cm/s, a typical conveyor speed in food processing. The velocity and acceleration of the platform were estimated from the first and second derivatives of the LAH_2 measurements using the second-order approximation (5), which are compared against the tachometer measurements and their derivatives.

System Identification and Sensor Computation Validation: To determine the system parameters (damping coefficient c and platform mass m_p), the free response (position) of the platform (without broiler $m_b = 0$) subject to an initial displacement of 0.15 m (6 inches) was recorded using LAH_2. The response and fitted models are given in Fig. 6. The parameters are calculated from Fig. 6 using the logarithmic decrement approach

$$\xi = \frac{\delta}{\sqrt{4\pi^2 + \delta^2}} \tag{11a}$$

where

$$\delta = \frac{1}{p} \ln \frac{x(t_1)}{x(t_{1+p})} \tag{11b}$$

where t_1 and t_{1+p} are the times at which the first and $(1+p)$th peak occurs. Hence

$$m_p = 2k \left(\frac{t_d}{2\pi} \right)^2 (1 - \xi^2) \tag{12a}$$

and

$$c = \frac{4\pi m_p \xi}{t_d \sqrt{1 - \xi^2}} \tag{12b}$$

where t_d is the damped period of the free response. The values of the parameters used in the subsequent experiments are summarized in Table V.

Fig. 7 shows the platform acceleration (on which the broiler sits) as a result of two different initial displacements (0.105 and 0.145 m). In both cases, model (10) was used to predict the platform acceleration. A comparison between the two corresponding acceleration as measured by LAH_2 shows that these measurements from the LAH sensors for the two different initial displacements follow the predicted acceleration. As expected, acceleration estimated from the derivative of the displacement data tends to be noisy.

Results and Discussions: The results obtained experimentally with live broilers are given in Figs. 8 and 9.

i) Effect of acceleration on broiler motion:

Fig. 8(a) and (b) compares the absolute displacement of the broiler subject to two different initial accelerations given in Fig. 7. Fig. 8(a) shows a close agreement between the platform displacement (x_p) and broiler displacement (x_o) when the initial displacement was 0.105 m. The experimental results for the larger acceleration (with $x(0) = 0.145$ m) suggest that slippage had occurred during the free response between the broiler and platform as evident in the deviation between the two displacement data sets in Fig. 8(b). A comparison of the measured acceleration from both LAHs reveals sustained periods of high acceleration rates (2 gs) which is especially apparent from the broiler data from Fig. 7. Such high acceleration rates not only promote slippage but also invoke a relatively large involuntary reaction from the startled broiler such as wing flapping and walking.

ii) Limiting velocity on vertical profile scanning:

Fig. 9 illustrates the effect of speed on the vertical profile by comparing two profiles scanned by the LAV as a live broiler on

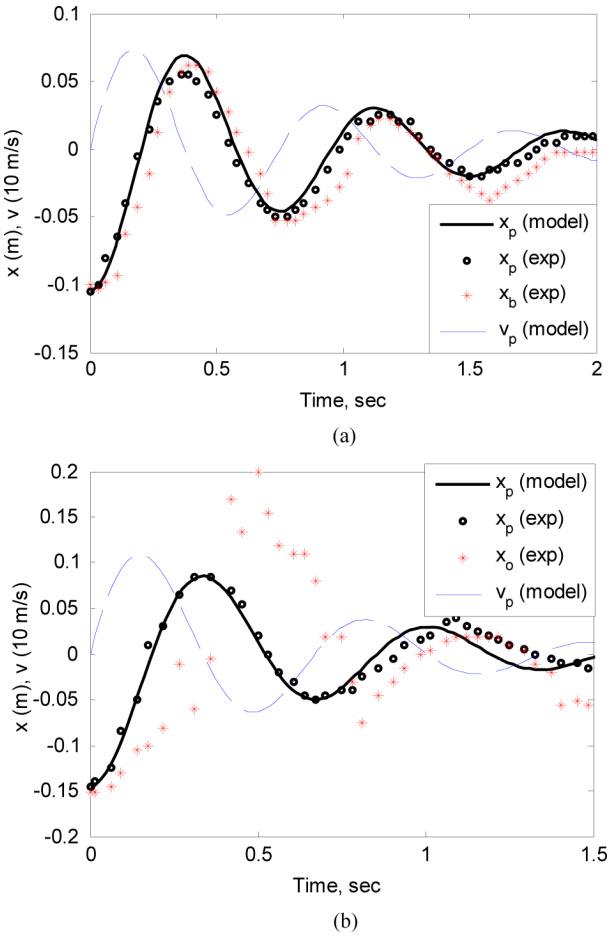

Fig. 8. Effects of acceleration. (a) $\mathrm{x}(0) = 0.105$ m, $\mathrm{v}(0) = 0$ m/s, (b) $\mathrm{x}(0) = 0.145$ m, $\mathrm{v}(0) = 0$ m/s.

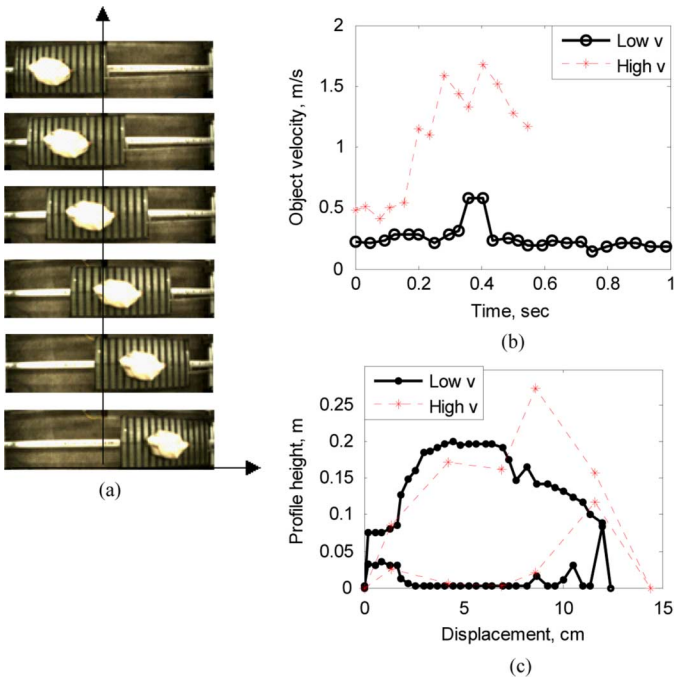

Fig. 9. Effects of high velocities in profile scanning. (a) Broiler motion. (b) Broiler velocity. (c) 2-D broiler boundary.

a platform moving through the LAH/LAV at two different velocities. The first velocity (that serves as basis for comparison)

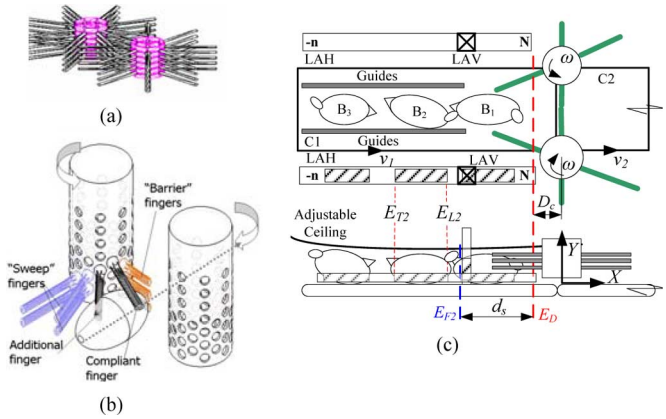

Fig. 10. Singulation process. (a) Passive singulator. (b) Active singulator. (c) Application of LAH/LAV sensor.

has been based on a line speed (of 0.30–0.46 m/s) commonly used in a typical poultry processing plant. The 2nd velocity was specially chosen at a much higher velocity (at 1.5 m/s). The detailed velocity profiles are shown in Fig. 9(b) and the corresponding 2-D broiler boundary as scanned by the LAV is shown in Fig. 9(c). It can be seen that the resolution of the 2-D profile has significantly deteriorated at high velocities. Hence, the effectiveness of the LAV sensors as a means of slip and feature detection on the object is highly dependent on relative size, r_s of the object feature of interest being measured, the sensor sampling time t_s, and the maximum velocity $v_{\max}$ of the object. We design the system such that the scanning resolution $v_{\max}t_s$ is less than the characteristic size r_s of the feature being detected. In (13), a factor 0.5 is used to ensure that this condition is met

$$v_{\max}t_s \leq 0.5r_s. \tag{13}$$

For $r_s = 0.025$ m and $v_{\max} = 0.3$ m/s, the minimum sampling time required is 41.7 ms.

General Remarks: The inherent motion of the platform tends to invoke relative motion and/or bodily movements of the broiler and such responses tend to exacerbate at higher platform velocities. This occurrence highlights the importance of the LAH to actively monitor and track the motion of the broiler as its vertical profile is being scanned by the LAV to ensure accurate construction of the 2-D broiler boundary. The importance of retrieving accurate 2-D profiles is reinforced from the example of estimating object transitions.

IV. Active Singulation Application

In high-speed food processing, natural objects (such as agricultural, poultry or meat products) must be singulated into equal spaces for repetitive operations executed mechanically. Since it is impractical to label or tag individual natural objects, noncontact optical LA sensors are a logical choice. Unlike a conventional singulator, as shown in Fig. 10(a), [1], [2] where a high density of fingers is rotated continuously, active singulation requires only a small number of finger-sets as illustrated in Fig. 10(b), which uses the LAH/LAV sensor feedback to synchronize the drum motion with the arrival of each object. Active singulation eliminates excess movement when the object is not completely in the specified region, and thus, active singulation has significant potentials in live-product handling applications.

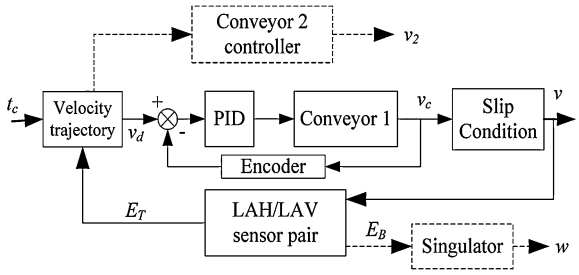

Fig. 11. LAH/LAV-based control scheme.

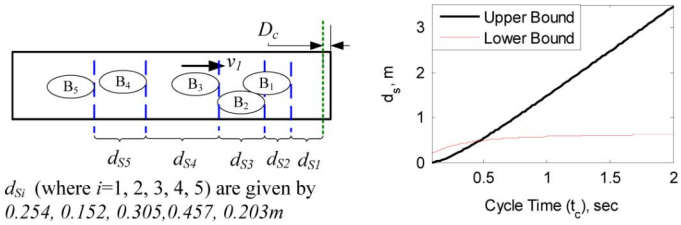

Fig. 12. Parameters used in simulation.

Fig. 10(c) shows an example singulation system, where broilers of varying spacing are fed into a singulator from the first conveyor (C1) and exit on the second conveyor (C2). The voluntary motion of the broiler is discouraged by the dark adaptation effects of a two-stage illumination system [20], as well as physically constrained by low ceiling and side panels on C1 such that broilers sit on the conveyor surface as they enter the singulator. These, along with the short cycle-time (in the order of 1 s), are bases for the assumption to neglect the lateral movements of the objects, which are restricted and relatively insignificant. The sensor pair uses the LAH to determine the spacing d_s between the object B_1 being singulated and the next incoming object B_2, and the LAV to detect the front edge of B_2. The singulating fingers execute when the front edge of B_1 reaches a critical distance D_c [from the centerline of the drums, as shown in Fig. 10(c)] allowing space to avoid collision with the barrier fingers on the drums. This position corresponds to E_D on the LAH. As B_1 is being singulated, the rotational motion of the drums will accelerate B_1 towards C2 creating a spacing between B_1 and B_2 immediately after which the LAV scans the B_2 as it passes through. The LAH/LAV data is then fed back to manipulate the velocity for controlling the conveyors and the singulating fingers; v_1, v_2 and ω.

For simplicity, we focus on the control scheme built around the conveyor C1, which has the dynamics given in (9), to illustrate the application of the LAH/LAV sensor pair for active singulation of the objects. The objective of the repetitive control scheme (Fig. 11) is to present an object sequentially to the singulator precisely at a specified cycle time of t_c second, where the desired velocity trajectory v_d is computed in real time as follows:

$$v_d(t) = d_x(E_D - E_T)/(t_c - t) \quad \text{for } 0 \le t < t_c. \tag{14}$$

As shown in Fig. 11, this desired object velocity is fed into the velocity controller of C1, the acceleration of which is continuously monitored to assess if slippage occurs between the object and conveyor surface using (6). When the object passes through the LAV, it triggers the rotation of the fingers onto C2. An example consisting of five unequally spaced objects (Fig. 12) has been simulated to illustrate the active singulation process described above. Practical operating limits of the C1 velocity put a bound on the object spacing (front edge to front edge) if the desired cycle time t_c is to be maintained. The maximum object spacing corresponds to the case when the conveyor is commanded to accelerate from the lowest velocity $v_{\min}$ (at the start of the cycle) immediately to highest velocity $v_{\max}$. Similarly, the minimum object spacing is bound by the opposite case when $v_C = v_{\max}$ at the start of the cycle and is commanded to $v_{\min}$ immediately. Taking into account the conveyor dynamics and object slippage, the conservative upper and lower bounds of the object spacing are

$$d_{\min} \le d_s \le d_{\max} \tag{15}$$

where

$$\frac{d_{\max}/\tau}{v_{\max} - v_{\min}} = \frac{(t_c/\tau)\, v_{\min}}{v_{\max} - v_{\min}} + \left[\frac{t_c - t_s}{\tau} + e^{-t_c/\tau} - e^{-t_s/\tau}\right] \tag{15a}$$

$$\frac{d_{\min}/\tau}{v_{\max} - v_{\min}} = \frac{(t_c/\tau)\, v_{\max}}{v_{\max} - v_{\min}} - \left[\frac{t_c - t_s}{\tau} + e^{-t_c/\tau} - e^{-t_s/\tau}\right] \tag{15b}$$

and

$$\frac{t_s}{\tau} = \begin{cases} 0, & \text{if } \mu g\tau \ge v_{\max} - v_{\min} \\ -\ln\left(\frac{\mu g \tau}{v_{\max} - v_{\min}}\right), & \text{otherwise} \end{cases} \tag{15c}$$

Using the values given below

$$\mu = 0.5; \tau = 0.25\ \mathrm{s}; v_{\max} = 2\ \mathrm{m/s}; \quad \text{and}$$
$$v_{\min} = 0.05\ \mathrm{m/s}$$

the upper and lower bounds of the object spacing as a function of desired cycle time are graphed in Fig. 12. It is noted that a cycle time of less than 0.5 s is not sustainable because of the first-order lag of the conveyor system. In addition, the conveyor C2 provides an additional degree of freedom to help meet the cycle time requirement if the object spacing on C1 exceeds the bound.

The location of the object at each time step is shown in Fig. 13(a) depicting the motion of each object during each of the five singulation cycles. The corresponding velocity and acceleration of the conveyor are shown in Fig. 13(b) and (c), respectively. In this simulation, the maximum velocity of the conveyor is capped at 2 m/s, and the minimum velocity is set at 0.05 m/s in order to avoid static friction of C1. As seen in Fig. 13(d), the object displacement does not decrease linearly as a result of the first order conveyor dynamics and slippage that occurs as a result of varying conveyor velocities. It is noted that the conveyor velocity increases as the object approaches E_D due to the decreasing magnitude of $(t_c - t)$ in (14).

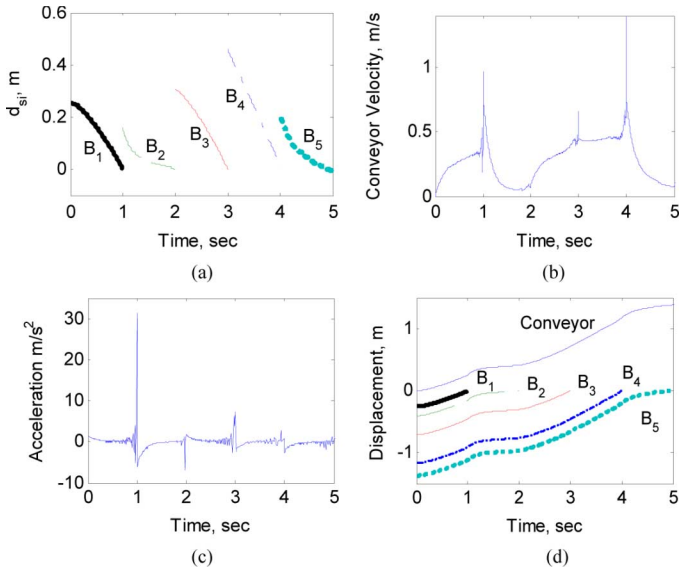

Fig. 13. Simulated results of active singulation ($t_c = 1$ s). (a) Object location. (b) Conveyor velocity. (c) Conveyor acceleration. (d) Object displacement.

V. Conclusion

We have presented a new sensing method based on the principle of a line array scanner to construct a 2-D profile of an object on a moving conveyor. This method utilizes a pair of line array sensors to capture the lateral profile as well as the velocity of the object. As illustrated with practical simulated and experimental examples, the lateral optical sensor exploits the fast scan rate of the photoelectric sensors to detect discrepancies between object position/velocity and conveyor position/velocity, which makes it a useful tool for applications where slip detection and compensation are required in real-time. Finally, we have also applied the lateral optical sensor for real-time velocity feedback and as a precise triggering device in an active singulation process.

Acknowledgment

The authors thank J. Jones of Hilco Inc., the staff of Banner Engineering Corporation, and TURCK Inc. for their help with the array scanners and communication hardware.

References

[1] K.-M. Lee, R. Gogate, and R. Carey, "Automated singulating system for transfer of live broilers," in *Proc. IEEE Int. Conf. Robot. Autom.*, Leuven, Belgium, May 1998, pp. 3356–3361.

[2] K.-M. Lee, "Design criteria for developing an automated live-bird transfer system," *IEEE Trans. Robot. Autom.*, vol. 17, no. 4, pp. 483–490, 2001.

[3] H. C. Garcia, J. R. Villalobos, and G. C. Runger, "An automated feature selection method for visual inspection systems," *IEEE Trans. Autom. Sci. Eng.*, vol. 3, no. 4, pp. 394–406, Oct. 2006.

[4] Y. Cheng and M. A. Jafari, "Vision-based online process control in manufacturing applications," *IEEE Trans. Autom. Sci. Eng.*, vol. 5, no. 1, pp. 140–153, Jan. 2008.

[5] K.-M. Lee, Q. Li, and W. Daley, "Effects of classification methods on color-based feature detection with food processing applications," *IEEE Trans. Autom. Sci. Eng.*, vol. 4, no. 1, pp. 40–51, Jan. 2007.

[6] Z. Du, M. K. Jeong, and S. G. Kong, "Band selection of hyperspectral images for automatic detection of poultry skin tumors," *IEEE Trans. Autom. Sci. Eng.*, vol. 4, no. 3, pp. 332–339, Jul. 2007.

[7] Y. Narita, S. Katahara, and M. Aoki, "Lateral position detection using side looking line sensor cameras," in *Proc. IEEE Intell. Veh. Symp.*, Columbus, OH, Jun. 2003, pp. 271–275.

[8] N. Galy, B. Charlot, and B. Courtois, "A full fingerprint verification system for a single-line sweep sensor," *IEEE Sensors J.*, vol. 7, no. 7, pp. 1054–1065, Jul. 2007.

[9] A. Nemecek, K. Oberhauser, G. Zach, and H. Zimmermann, "Distance measurement line sensor with PIN photodiodes," in *Proc. 5th IEEE Conf. Sensors*, Daegu, Korea, Oct. 2006, pp. 275–278.

[10] Kadowaki, K. Kobayashi, and K. Watanabe, "Rotation angle measurement of high-speed flying object," in *Proc. Int. Joint Conf. SICE-ICASE*, Busan, Korea, Oct. 2006, pp. 5256–5259.

[11] A. N. Belbachir, K. Reisinger, G. Gritsch, P. Schön, and H. Garn, "Automated vehicle velocity estimation using a dual-line asynchronous sensor," in *Proc. IEEE Intell. Transp. Syst. Conf.*, Seattle, WA, Oct. 2007, pp. 552–557.

[12] G. Reina, L. Ojeda, A. Milella, and J. Borenstein, "Wheel slippage and sinkage detection for planetary rovers," *IEEE/ASME Trans. Mechatronics*, vol. 11, no. 2, pp. 185–195, Apr. 2006.

[13] K. Herzog, E. Schulte, M. A. Atmanand, and W. Schwarz, "Slip control system for a deep-sea mining machine," *IEEE Trans. Autom. Sci. Eng.*, vol. 4, no. 2, pp. 282–286, Apr. 2007.

[14] T. Watanabe and M. Yamashita, "A novel anti-slip control without speed sensor for electric railway vehicles," in *Proc. 27th Annu. Conf. IEEE Ind. Electron. Soc.*, Denver, CO, Dec. 2001, vol. 2, pp. 1382–1387.

[15] C. Melchiorri, "Slip detection and control using tactile and force sensors," *IEEE/ASME Trans. Mechatronics*, vol. 5, no. 3, pp. 235–243, Sep. 2000.

[16] "A-GAGE® EZ-ARRAY™ series," *Banner Engineering Sensor Products Brochure*, pp. 288–290.

[17] "A-GAGE® high-resolution MINI-ARRAY® series," *Banner Engineering Sensor Products Brochure,* pp. 291–295.

[18] *BL20 Programmable Ethernet Gateway*, BL20, Turck Inc., Turck BL20-User Manual for Modbus TCP.

[19] *BL20 Analog Input Module*, BL20, Turck Inc., Turck BL20-I/O-Modules Hardware and Engineering.

[20] K.-M. Lee, J. Joni, and X. Yin, "Imaging and motion prediction for an automated live-bird transfer process," in *Proc. ASME Dynamic Syst. Control Division*, Orlando, FL, Nov. 2000, pp. 181–188.

Kok-Meng Lee, (F'05) received the M.S. and Ph.D. degrees in mechanical engineering from the Massachusetts Institute of Technology, Cambridge, in 1982 and 1985, respectively.

Since 1985, he has been with the Faculty of Mechanical Engineering, Georgia Institute of Technology, Atlanta. As a Professor of Mechanical Engineering, his research interests include system dynamics and control, machine vision, robotics, automation, and mechatronics.

Dr. Lee is a Fellow of ASME. He has held representative positions within the IEEE Robotics and Automation Society (RAS): he was an Associate Editor of the IEEE Transactions on Robotics and Automation (1994–1998), *RAS Magazine* (1994–1996), and the IEEE Transactions on Automation Science and Engineering (2003–2005), and Editor for the IEEE/ASME Transactions of Mechatronics (1995–1999). He served as Chair or Co-Chair for numerous international conferences. Recognitions of his research contributions include the NSF Presidential Young Investigator (PYI) Award, the Sigma Xi Junior Faculty Award, the International Hall of Fame New Technology Award, Woodruff Faculty Fellow, three Best Paper Awards and seven patents. He is also recognized as advisor for seven Best Student Paper Awards and a Best Thesis Award.

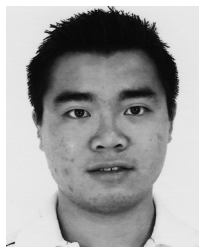

Shaohui Foong, (S'06) received the B.S. and M.S. degrees in mechanical engineering from the George W. Woodruff School of Mechanical Engineering, Georgia Institute of Technology, Atlanta, in 2005 and 2008, respectively. He is currently working towards the Ph.D. degree in mechanical engineering at the George W. Woodruff School of Mechanical Engineering, Georgia Institute of Technology, Atlanta.

His research interests include system dynamics/control, distributed sensing, sensor fusion, and automation.